High-Temperature Transformation of Graphite Coating on Silica Surface under Continuous Laser Radiation

Vladislav A. Kamensky[1*], Nadia M. Khamaletdinova[2], Diana G. Fukina[3], and Vladimir I. Bredikhin[1]

[1] Federal Research Center A.V. Gaponov-Grekhov Institute of Applied Physics of the Russian Academy of Sciences, 46 Ulyanov Str., Nizhny Novgorod 603950, Russian Federation

[2] G. A. Razuvaev Institute of Organometallic Chemistry of the Russian Academy of Sciences,49 Tropinin Str. , Nizhny Novgorod 603952, Russian Federation

[3] Lobachevsky State University of Nizhny Novgorod, 23 Gagarin Pr., Nizhny Novgorod 603950, Russian Federation

*e-mail: vlad340@ipfran.ru

Abstract. The physicochemical transformation of a graphite coating on silica glass (fiber and plate), when heated in air by micrometer wave laser radiation with a power of several kW/cm^2 with temperature up to 2500 K at which optical transmission increases from zero to 10% (UV range) and up to 40% (IR range), was detected. Based on a complex of the conducted studies, it was concluded that, along with elimination of part of absorbing species, the graphite powder of the coating as well as silicon dioxide and atmospheric oxygen present in its composition transform to others, transparent compounds: silica, silicon carbide SiC, and presumably (tri)(di)carbonates transparent in UV-VIS up to ~5 eV. Until recently, (tri)(di) carbonates of silicon were known mainly from theoretical works. The high-temperature coating consists of residual graphite, which allows laser heating, and C-O-Si compounds, including carcinogenic SiC at a level of ~2 10−6 mg.

Keywords: laser scalpel; semiconductor laser; silica fiber; light absorbing coating; high temperature stabilization; physicochemical transformation of coating materials; silica carbonates.

Paper #9376 received 14 Oct 2025; revised manuscript received 21 Nov 2025; accepted for publication 23 Nov 2025; published online 29 Dec 2025. doi: 10.18287/JBPE25.11.040307.

1 Introduction

The study of material properties at temperatures of about 2500 K and the development of methods for synthesizing new materials are still highly relevant. Indeed, phase transitions of many important materials such as silicon carbide, diamond, quartz, a number of nonlinear optical, laser materials occur in this temperature region. Information on key parameters in this critical region is neither accurate nor reliable [1]. The same concerns both, developing technology production of traditional materials (quartz silicon carbide, diamond) [2−6,7,8] and searching for methods of obtaining new materials, for example, silicon (tri)(di)carbonates [9−12] and carbon-nitride materials [13]. A number of issues associated with solar hydrogen energy and CO_2 reduction in the atmosphere are related to this field of research [9-12, 14]. A number of works on producing materials under shock high-temperature conditions using pulsed lasers appeared in the last decay [15−19].

Recently, this problem has attracted researcher attention due to the advent of laser sources capable of creating a high radiation density of up to several kW/cm^2 in continuous mode without preliminary focusing, for example, semiconductor lasers with a fiber-optic silica output. It was found that, when a light-absorbing coating is applied to the tip (diameter ~0.5 mm) of a fiber of a semiconductor laser with a fiber-optic output (laser scalpel) promising for use in medical practice [15], the tip is heated in air to high temperatures (up to ~2500 K initially with next stabilization to ~1800 K) [21, 22]. This opened up new opportunities for laser surgery, in particular, for the treatment of urolithiasis [23,24] and malignant tumors [25]. The maximum temperature of the new point tool is determined by the temperature stability of silica that is used as a fiber material.

Laser surgery mainly uses fiber optic lasers, the cleaned tip of the quartz fiber acts as the cutting element [26, 27], whereas obtaining newly emerging chemical compounds as a result of high temperature processes

require additional study, for example, in terms of cancerogenity. Therefore, from the point of view of toxicology, the study of high-temperature interaction of a silica fiber with a carbonized biotissue is important, especially in connection with the use in laser surgery of highly absorbing coatings, graphite being one of their components. The possibility of producing high-temperature objects with high temperature and pressure gradients is apparently associated with the recent reports on microdiamonds synthesized by laser and other methods with similar physical parameters [18, 19], on synthesized silicon carbide, carbide based ceramics and oxide based ceramics in silicone resins [28]. It is very interesting to study in more detail the phenomena occurring in materials of a light-absorbing layer heated by absorbed laser radiation [21, 22], both for applications of such fibers in medical practice and, in a broader field of high-temperature physics, for the search for new high-temperature materials and the improvement of production technologies for materials such as diamond, silicon carbides, etc. using new laser devices as sources of high-power controlled local heating.

Animal experiments [25] demonstrated the potential of the new instrument. Experimental lithotripsy procedures on real patients also proved successful [23 ,24]. However, concerns about the safety of the high-temperature instrument based on a graphite-silicone coating regarding its carcinogenic potential arose. Indeed, at high temperatures (up to ~2500 K) during the production of high-temperature coatings, the starting materials form new products whose carcinogenic properties should be studied. One such product may be SiC, which is classified as a hazard class 4 [29]. Considering the extreme conditions of obtaining a high-temperature coating, the possibility of the formation of other compounds cannot be ruled out. The goal of this work is to determine the chemical composition of the products and the chemical processes under extreme temperature and radiation loads occurring when the silica fiber tip in contact with a graphite coating containing organosilicon substances is exposed to high-power IR radiation. For this purpose, we use the methods of UV-VIS and IR spectroscopy, optical microscopy, X-ray spectroscopy (X-ray powder diffraction), scanning electron with X-ray microanalysis microscopy, and analytical balance.

2 Equipment and Methods

The following equipment was used in the study: Lakhta-MilonTM lasers (Russia, Saint-Petersburg) with fiber-optic output and wavelengths of 1.315; 0.97 and 0.81 μm; Shimadzu UV-1800 spectrophotometer (Japanize, Tokio); FSM 1201 FT-IR spectrometer; Nikon Eclipse CI-1800 microscope ; XRD diffractometers, including Shumadzu XRD-6100 diffractometer, CuKα 1 operating in 10−60 deg, 2 deg/min mode; scanning electron microscope JSM-IT300LV(JEOL, Japanize, Tokio) with electron beam diameter of about 5 nm at a probe current of less than 0.5 nm; elemental

X-ray microprobe analyzers with X-MaxN 20 detector (OxfordInstruments, USA); and Shirko VIBRA AJH-CE analytical balance, accuracy 1 mg.

The high color temperature of a laser heated object was determined from measurements of the emission spectrum of the heated coating with the Ocean Optics QE65Pro spectrometer (USA) in the range of 400–800 nm. Accuracy is approximately 20 K.

The object under study was a high-temperature graphite coating applied to the output tip of a silica fiber of a semiconductor laser, or to the surface of a silica-glass optical plate heated by absorbing IR radiation from the semiconductor laser (the effect is virtually independent of wavelength). The coating application technology, in brief, consists in applying a drop of graphite powder emulsion in silicon varnish to the distal end of the fiber or the optical silica plate. The varnish with graphite powder is dried at a temperature of several hundred degrees K and then heated by laser radiation up to ~1000 K. Note that the coating is colored black. Next, the laser power is increased (up to ≥ 1 W in the case of the fiber). The coating temperature rises sharply, the tip is visualized as flashes of white light, then within ~ 1 s the glow intensity decreases and the temperature self-stabilizes at ~1800 K. As a result, the coating structure changes and becomes grey after cooling [21,22]. Clearly, this is connected with the processes in the coating and in the fiber material, as a result of which physicochemical transformations of the coating composition can occur.

In what will follow, we will present the results of physicochemical studies of the structure and composition of the obtained coating.

3 Results

3.1 Microscopy

Primary microscopic data on the structure of the coating immediately on the fiber tip (diameter of about 0.5 mm) show the change in its color from black to grey [21]. Since investigation of such a specific sample is rather difficult, a few optical studies were carried out on a model, analogue sample. A coating of the same composition was applied to an optical silica plate as ~ 9 cm^2 area spot; the model sample was exposed to the radiation from the same laser using a piecewise raster technique with a laser beam defocused by 1.5–2 times with a corresponding power increase (Fig. 1). Thus, the temperature regime for obtaining an analog coating on silica (ACS) remained almost the same as for the fiber. The dried, non-irradiated coating on the silica plate (spot 1) and after irradiation (spots 2 and 3) is shown in Fig. 1. The spot 2 was preheated at a laser power of 100 W/cm^2 (T < 1000 K, the spot remained black) and then annealed at a power of 400 W/cm^2 in the high-temperature glow mode (T = (2500, 1800) K). The spot 3 was annealed at a power of 600 W/cm^2 without preheating. No ablated light-absorbing particles were detected during the high-temperature annealing (T ≈ (2500, 1800 K), but the mass of the coating decreased by 2−3 times.

Fig. 1 (1) Absorbing coating on silica plate. Dried (~ 300 K) drop; (2) dried, heated at 100 W/cm^2 (T ~ 1000 K) and annealed at 400 W/cm^2 (T ~ 2000 K); (3) dried at room temperature and annealed at 600 W/cm^2 (T ~ 2000 K).

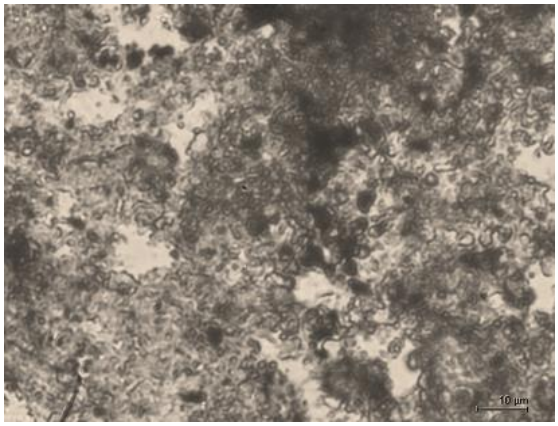

Fig. 2 ACS microstructure.

The ACS microstructure after annealing is shown in Fig. 2. The coating has a rather inhomogeneous transparency and density of microparticle components.

3.2 UV-VIS Spectroscopy

The UV-VIS transmission spectra obtained for the sample at different stages are presented in Fig. 3: 1 – the sample dried at room temperature, 2 – dried at room temperature and exposed to a temperature of ~1000 K, 3 – dried at room temperature and irradiated by a laser at a power of 6 W (T ~ 2000 K), 4 – dried at room temperature, irradiated by 1W laser (T ~ 1000 K) plus exposed to 6 W radiation (T ~ 2000 K); 5 – transmission spectrum of dried silicon varnish.

Obviously, during high-temperature laser treatment the transmission increases from 0 to 40% at the laser wavelength and smoothly decreases to 15% in the ultraviolet region. The drop at absorption at a wavelength of 1 μm explains the temperature stabilization effect [21]. The drop at absorption in a wide region indicates ablation of most of the graphite from the irradiated region and the transition of the remaining graphite and other coating components to secondary chemical forms with band-gap energies of 3–5.5 eV. The residual absorption is apparently determined by the remains of graphite and uncontrolled impurities. The regular increase in losses with a decrease in wavelength is most likely due to light scattering on a polydisperse coating. Based on the available literature data [28], it was assumed that silicon dioxide SiO_2 and silicon carbide SiC can be formed as a result of decomposition of silicon varnish under high-temperature (up to ~ 1000°C) conditions. On the other hand, SiO_2 (the fiber and the glass substrate are also SiO_2) interacts with graphite C at temperatures of 1600–2500 °C following the known reaction $SiO_2 + 3C \rightarrow SiC + 2CO\uparrow$ to yield silicon carbide SiC. SiC microcrystals were observed, for example, in a silicon film irradiated with femtosecond laser pulses in the transparency band (λ = 522 nm) [28]. The band gap of SiC is known to be ~ 3 eV [29–31]. The possibility of diamond formation under similar conditions was speculated in Refs. [18,19,28].

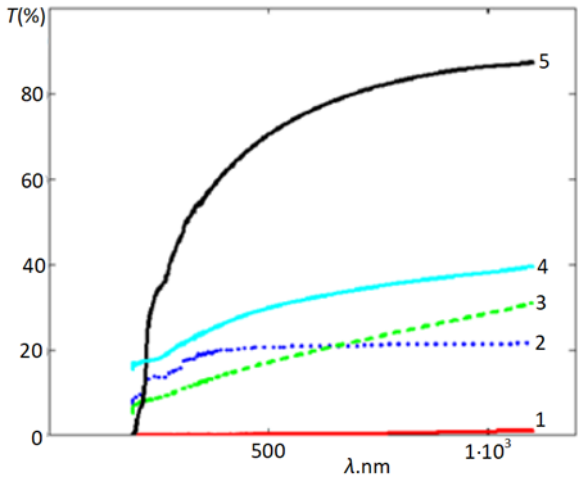

Fig. 3 Transmission spectra of silica plate with light absorbing layer: 1 – dried drop of graphite in silicon varnish, 2 – drop irradiated by 1 W laser, 3 – irradiated by 6 W laser; 4 – drop exposed to 1W laser plus irradiated by 6 W laser; 5 – dried layer of silicon varnish.

Further studies (UV-VIS-IR spectral, X-ray structural, electron and optical microscopic) were carried out with ACS powder obtained by scraping the coating from a silica plate produced by the method described above. A typical micrograph of the powder with single transparent microcrystallites is shown in Fig. 4.

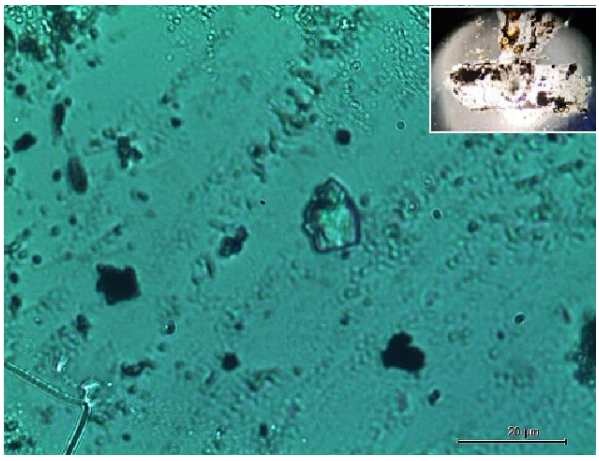

Fig. 4 Photomicrograph of microscraping on object-plate. Shadow mode. Inset: crystalline aggregate (~10 μm diameter).

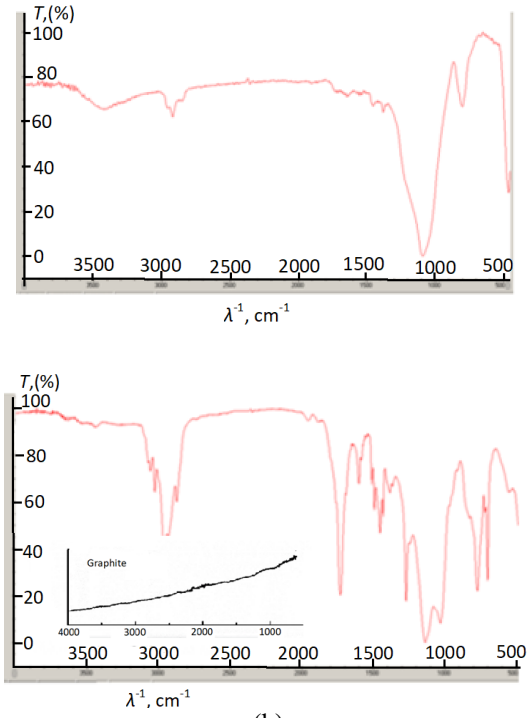

(b)

Fig. 5 IR transmission spectrum of ACS powder in KBr pellet (a) and of silicon varnish film on KBr window dried at 200 °C (b). Inset in Fig. 5b shows typical graphite IR spectrum [32].

3.3 IR Spectroscopy

An IR transmission spectrum obtained on ACS powder in a KBr tablet is shown in Fig. 5a. IR spectra of the samples were measured on a FTIR "FSM 1201" spectrometer (Russia) in the 400–4000 cm^{-1} wavenumbers range at the resolution of 4 cm^{-1} using the KBr pellet. Peak wavenumber accuracy is 0.25 cm^{-1}. Figure 5b shows the spectra of raw materials: silicon varnish on the KBr window dried at T = 200 °C and graphite (Inset) [33].

The absorption bands at 3500 and 3000 cm^{-1} are due to the presence of impurities in the parent KBr powder (Fig. 5a), and the rest to the powder under study. According to the literature, the 1075, 750, and 480 cm^{-1} bands belong to the Si-O and C-O bonds and their associates [34, 35], including amorphous SiO_2 [35, 36]. The main characteristic absorption bands of SiC are also located in the 500 cm^{-1} and 800 cm^{-1} regions [7]. The analysis of the results of IR absorption spectra does not contradict the presence of silicon carbide SiC in the powder-scraping, but draws attention to the fact that the highest absorption intensity in the spectrum is observed in the 1050 cm^{-1} region, which corresponds to oxygen containing silicon and carbon compounds. Amorphous SiO_2 makes a significant contribution to the ACS powder IR spectra.

3.4 X-Ray Powder Diffraction

The obtained compounds were measured with a Shumadzu XRD-6100 diffractometer featuring CuKα1 rays in a scanning mode of 10–60°, 2°/min. The measurements were made in a 0.5 mm thick aluminum cuvette. The XRD spectra for two portions of ACS powder obtained in independent experiments are presented in Fig. 6 a, b. The used graphite was also measured (Fig. 6 c).

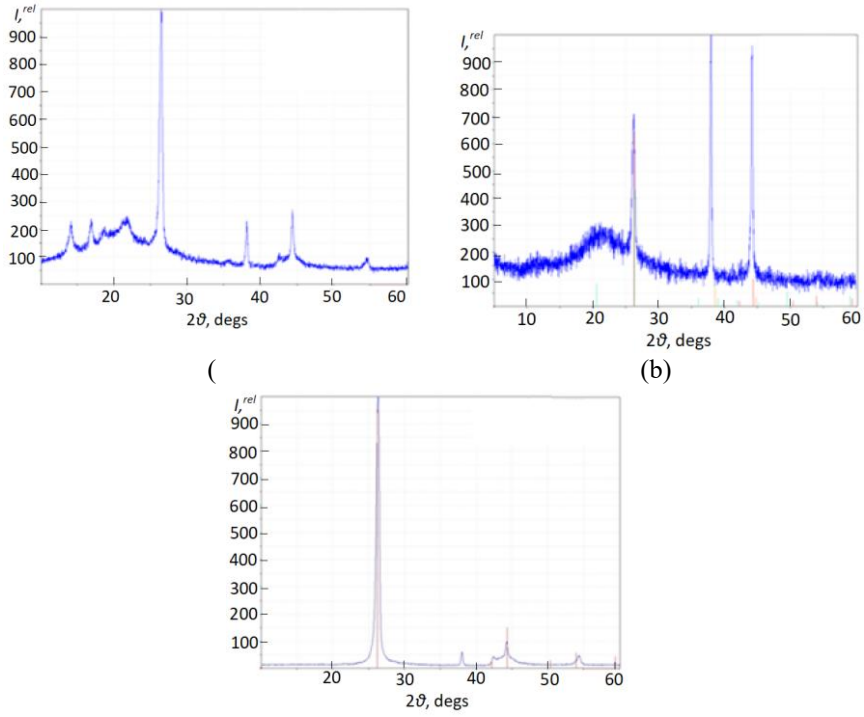

((b)

(c)

Fig. 6 XR diffractograms of (a, b) ACS product and of (c) graphite powder.

Graphite is present in all samples. In the first measurement (Fig. 6 a), the graphite lines in the powder demonstrate 100% coincidence with the graphite powder (c), both in the angle and qualitatively in the ratio of peak intensities. There is only a small hint to an additional line at about 38°. In Fig. 6 b, the main lines at first sight repeat Fig. 6 a. However, the ratio of the peaks is significantly different. The first peak at 26°, leading in the first measurement, becomes noticeably smaller than the second and the third ones, the ratio of the intensities of the 2-nd and 3-rd peaks also changes to the opposite. It can be concluded that in the second X-ray diffraction pattern, the proportion of graphite decreases significantly and there appears the contribution of another compound. This compound may be SiC, the XRD lines of which in the range of 35–60° are close to the corresponding ACS lines [8], and the intensity ratio corresponds to the observed differences.

A distinct band ($2\theta = 22°$) corresponding to amorphous compounds with Si-O bonds is observed in all XRD spectra of the ACS powder [37]. Further, two reflexes at 14 and 17° are clearly visible in the first XRD. No explanation for these bands has been found in the literature. The discussion will be presented below.

3.5 Scanning Electron Microscopy Studies with X-ray Microanalysis

The images of the micropowder structure (Fig. 7 a–c) of the ACS product were obtained by scanning electron microscopy (SEM) with a JSM-IT300LV microscope (JEOL) having an electron beam diameter of about 5 nm and a probe current below 0.5 nA. The surface topography of the samples was studied using low-energy secondary electrons and backscattered electrons. The elemental composition (Fig. 7 a–d, Table 1) of the samples was studied using X-ray microprobe analysis (XMP) with X-MaxN 20 detector (Oxford Instruments). The error depends on the element and its concentration in the mixture. For concentrations of 0.1−1 mass%, the absolute error is 0.03−0.25, for concentrations of 1−5 mass%, the absolute error is 0.02−0.75, for concentrations of 5−12 mass%, the absolute error is 0.5−1.2, and for concentrations above 12−15%, the absolute error is 1−3. For light elements–at similar concentrations, the error is 1.5−2 times higher.

An example of general picture with marked sites of elemental composition measurements is shown in Fig. 8 a, an example of carbon distribution in Fig. 8 b, a silicon distribution in Fig. 8c, and an example of oxygen distribution is illustrated in Fig. 8 d.

The comparison of the photomicrographs in Fig. 7 and in Fig. 2 shows the internal structure of the particle – a cellular, dendrite-type structure appeared in the photos in Fig. 8. It should be noted that the Si and O distributions coincide in the element distribution maps (Fig. 8 c, d).

Judging by the element distribution maps, the sample has a heterogeneous composition (Fig. 8a). Two distinctive areas can be distinguished:

1) high (predominant) carbon content (Fig. 8 b);
2) high silicon and oxygen content (Fig. 8 c and 8 d).

The composition of these phases was measured individually (Table 1).

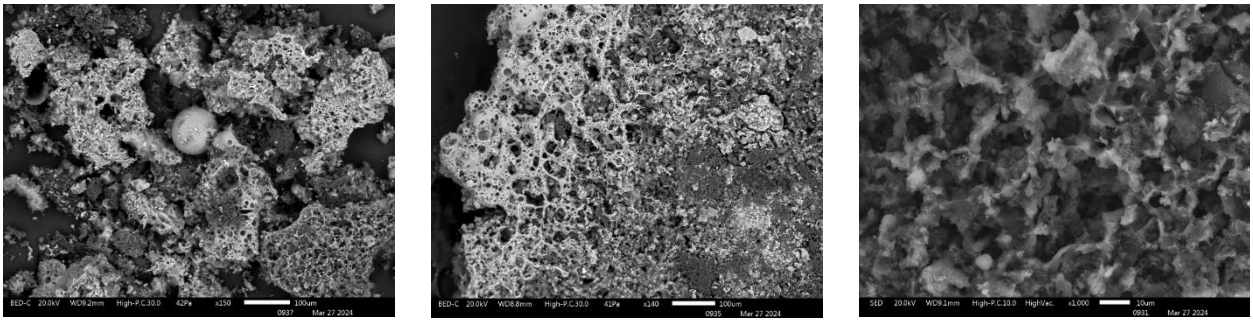

Fig. 7 Scanning electron photomicrographs of the surface of ACS powder particles: (a) separate particles, (b) dendrite-type, (c) pore-type structures.

Table 1 The elemental composition in atomic fractions at the points highlighted in the electron image in Figs. 2 (a−d).

Spectrum	C (atomic fraction)	O (atomic fraction	Si (atomic fraction)	Area
Spectrum 281	4.132	2.369	0.446	(2)
Spectrum 282	4.518	2.239	0.354	
Spectrum 283	7.184	0.733	0.073	(1)
Spectrum 284	7.267	0.686	0.065	
Spectrum 285	7.151	0.752	0.077	

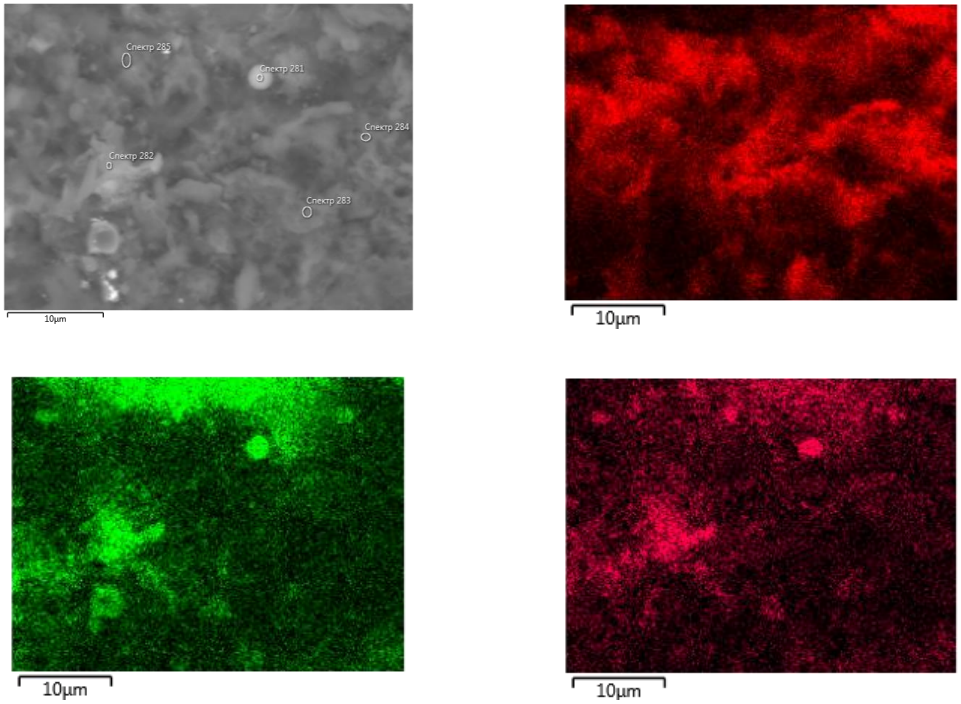

Fig. 8 Electron images of element distribution maps: (a) general, (b) carbon, (c) silicon, and (d) oxygen.

In area (2), the Si to O ratio does not correspond to silicon oxide SiO_2, since there is much less silicon, while there is a noticeable amount of carbon. Carbon can be either part of the Si-O-C compound or a background signal from area (1).

In area (1), oxygen and silicon are detected besides carbon. The Si to O ratio does not correspond to silicon oxide SiO_2 either, since there is much less silicon. Here we have a phase of pure C or a combination of C and O.

The Si to C ratio in both areas does not correspond to silicon carbide SiC, there is much more carbon. No other impurities were detected within the method sensitivity (0.1 mass%). An increased error in determining the amount of carbon and oxygen (up to 5%) due to the low energy of their X-ray radiation was noted.

Measurements of the coating's atomic composition show that it consists primarily of carbon, silicon, and oxygen. Silicon, the presence of which determines the formation of the high-temperature solid Si-C-O compound, has the lowest concentration. Carbon, in the form of graphite, is introduced during the coating process and determines the residual optical absorption of laser pump radiation. Therefore, the silicon concentration can be used to estimate the potential mass of Si-C-O compounds in the coating. Based on the total mass of the ~~s~~calpel tip coating of ~ $2 \cdot 10^{-3}$ mg (according to micro-weighing of samples) and the relative concentration of silicon, it can be estimated that the tip mass of Si-C-O compounds is ~$2 \cdot 10^{-4}$ mg. The first result is that the seemingly obvious expectation of the presence of silicon carbide (SiC) is not met. If it is present, its tip content does not exceed a few percent of the silicon atom concentration, i.e., no more than ~2 10^{-6} mg. This result allays concerns about the hazards of SiC, but raises questions about the residual mass of the coating. The very high oxygen concentration indicates the possible presence of compounds such as silicon carbonates SiO_2CO_2, $SiO_2(CO_2)_2$, and $SiO_2(CO_2)_3$. Information on such compounds, and especially on their potential hazards, is currently extremely limited in the literature.

4 Conclusions

The physicochemical properties of the carbon – silicon coating of the laser scalpel tip in result of laser high temperature heating were studied. It was found that:

- As the temperature is stabilized, the UVI-VIS absorption of initial black carbon-silicon varnish layer drops sharply, the transmission at a wavelength of 1 μm increases from 0 to 40%. The transparency window from ~0.2 μm to ~1 μm is observed. It corresponds to the effective band gap of the coating materials of ~3–5 eV.
- The high-temperature coating consists of residual graphite, which allows laser heating, amorphous SiO_2, and C-O-Si compounds mainly. Significant amounts of oxygen have been shown to be present in the resulting lesion. Amount of carcinogenic SiC does not exceed of ~2 10^{-6} mg.
- We have hypothesized that high-temperature crystalline C-O-Si compounds with a band gap of up to 5 eV such as silicon (tri)(di)carbonates are present in the coating. The properties of such compounds, in particular their carcinogenicity, require further study.

Conflicts of Interest

The authors declare no conflict of interests.

Acknowledgments

This work was carried out under financial support of the Ministry of Science and Higher Education of the Russian Federation, project FFUF-2024-0030.

The IR study was supported by the Ministry of Science and Higher Education of the Russian Federation within the State Task using the equipment of the Analytical Center of the G.A. Razuvaev Institute of Organometallic Chemistry, Russian Academy of Sciences.

The XRD and SEM studies were implemented on the equipment of the Collective Usage Center "New Materials and Resource-saving Technologies" (Lobachevsky State University of Nizhnii Novgorod).

We thank N. M. Bityurin, O.V. Kuznetsova and M.A. Lopatin for discussions.

References

1. G. V. Belov, A. O. Erkimbaev, V. Y. Zitserman, G. A. Kobzev, and I. V. Morozov, "Experience of thermophysical database development using modern Information technologies (Review)," High Temperature 58, 566–582 (2020).
2. R. G. Yalman, J. F. Corwin, "Hydrothermal Reactions under Supercritical Conditions. III. The Effect of pH on the Crystallization of Silicon Dioxide" The Journal of Physical Chemistry 61(10), 1432–1437 (1957).
3. P. S. De Carli and J. C. Jamieson, "Formation of an amorphous form of quartz under shock conditions" The Journal of Chemical Physics 31(6), 1675–1676 (1959).
4. H. P. Martin, R. Ecke, and E. Müller, "Synthesis of nanocrystalline silicon carbide powder by carbothermal reduction," Journal of the European Ceramic Society 18(12), 1737–1742 (1998).
5. C. L Frewin, C. Coletti, J. J. Register, M. Nezafati, S. Thomas, and S. E. Saddow, "Silicon carbide materials for biomedical applications," in Carbon for Sensing Devices, D. Demarchi, A. Tagliaferro (Eds.), Springer, Cham, 153–207 (2015). Online ISBN: 978-3-319-08648-4
6. G. Q. Liang, H. Qian, Y. L. Su, L. Shi, Q. Li, and Y. Liu, "Review of solution growth techniques for 4H-SiC single crystal," China Foundry 20, 159–178 (2023).
7. S. A. Grudinkin, V. G. Golubev, A. V. Osipov, N. A. Feoktistov, and S. A. Kukushkin, "Infrared spectroscopy of silicon carbide layers synthesized by the method of atomic substitution on the surface of single-crystal silicon," Physics of the Solid State 57, 2543–2549 (2015).
8. D. O. Moskovskikh, L. Ya-Cheng, A. S. Rogachev, P. J. McGinn, and A. S. Mukasyan, "Spark plasma sintering of SiC powders produced by different combustion synthesis routes," Journal of the European Ceramic Society 35, 477–486 (2015)
9. A. Burchert, S. Yao, R. Müller, C. Schattenberg, Y. Xiong, M. Kaupp and M. Driess, "An Isolable Silicon Dicarbonate Complex from Carbon Dioxide Activation with a Silylone," Angewandte Chemie International Edition 56(7), 1894–1897 (2017).
10. R. Zhou, B. Qu, J. Dai, and X. C. Zeng, "Unraveling Crystalline Structure of High-Pressure Phase of Silicon Carbonate Rulong Zhou," Physical Review X 4, 011030 (2014).
11. M. Santoro, F. Gorelli, J. Haines, O. Cambon, C. Levelut, and G. Garbarino, "Silicon carbonate phase formed from carbon dioxide and silica under pressure," Proceedings of the National Academy of Sciences 108(19), 7689–7692 (2011).
12. K. Watanabe, H. Kato, and Y. Matsumoto, "Effective Conversion of CO_2 to Carbonate in Surface Oxidation Processes at Si(100)," The Journal of Physical Chemistry B 102(41), 8042–8048 (1998).
13. Y. Wu, Y. Chen, C. Ma, Z. Lu, H. Zhang, B. Mortazavi, B. Hou, Ke Xu, Haodong Mei, T. Rabczuk, H. Zhu, Z. Fang, R. Zhang, and C. M. Soukoulis, "Monolayer C_7N_6: Room-temperature excitons with large binding energies and high thermal conductivities," Physical Review Materials 4, 064001 (2020).
14. G. Zini, P. Tartarini, Solar Hydrogen Energy Systems, Springer Milano (2012). eBook ISBN: 978-88-470-1998-0
15. R. He, N. Zhou, K. Zhang, X. Zhang, L. Zhang, W.Wang, and D. Fang, "Progress and challenges towards additive manufacturing of SiC ceramic," Journal of Advanced Ceramics 10, 637–674 (2021).
16. S. Meyers, L. D. Leersnijder, J. Vleugels, and J.-P. Kruth, "Direct laser sintering of reaction bonded silicon carbide with low residual silicon content," Journal of the European Ceramic Society 38(11), 3709-3717 (2018).
17. J. T. Eddy, Microfabrication of Silicon Carbide and Metallized Polymers Using a Femtosecond Laser, Theses and Dissertations, Brigham Young University (2023).
18. V. I. Yusupov, V. M. Chudnovskii, and V. N. Bagratashvili, "Laser-induced hydrodynamics in water-saturated biotissues: 2. Effect on delivery fiber," Laser Physics 21, 1230–1234 (2011).
19. Y. Gong, D. Luo, M. Choe, Y. Kim, B. Ram, M. Zafari, W. K. Seong, P. Bakharev, M. Wang, I. K. Park, S. Lee, T. J. Shin, Z. Lee, G. Lee, and R. S. Ruoff, "Growth of diamond in liquid metal at 1 atm pressure," Nature 629, 348–354 (2024).
20. J. Chen, "Research on applications of semiconductor laser in medical fields," Proceedings of the 3rd International Conference on Mechanical Engineering and Intelligent Systems (ICMEIS 2), Atlantis Press, 29–32 (2015).
21. V. Bredikhin, "Optothermal properties of a converter of laser radiation to the radiation of a high-temperature point source," Materials Research Express 6(6), 065412 (2019).

22. V. Bredikhin, V. Kamensky, N. Sapogova, V. Elagin, M. Shakhova, L. Snopova, and N. Bityurin, "Indirect laser surgery," Applied Physics A 122(3), 181 (2016).
23. O. S. Streltsova, V. V. Vlasov, E. V. Grebenkin, A. E. Antonyan, V. V. Elagin, V. F. Lazukin, N. I. Ignatova, and V. A. Kamensky, "Controlled Fragmentation of Urinary Stones as a Method of Preventing Inflammatory Infections in the Treatment of Urolithiasis (Experience in Successful Clinical Use)," Modern Technologies in Medicine 13(3), 55 (2021).
24. O. S. Streltsova, E. V. Grebenkin, N. M. Bityurin, V. I. Bredikhin, V. V. Elagin, V. V. Vlasov, and V. A. Kamensky, "Diode laser lithotription technique based on optothermal converter," Photonics 8(10), 452 (2021).
25. V. V. Elagin, M. A. Shakhova, M. A. Sirotkina, A. V. Shakhov, N. P. Pavlova, L. B. Snopova, V. I. Bredikhin, and V. A. Kamensky, "Can "indirect" contact laser surgery be used for fluorescence image guided tumor resections? Preliminary results," Technology in Cancer Research & Treatment 17, 1533033818805715 (2018).
26. A. T. Gursel, "Fiber Lasers and Their Medical Applications," Chapter 5 in Optical Amplifiers - A Few Different Dimensions, P. K. Choudhuryn (Ed.), IntechOpen (2018). eBook ISBN: 978-1-83881-480-9
27. K. Stock, T. Stegmayer, R. Graser, W. Förster and R. Hibst, "Comparison of different focusing fiber tips for improved oral diode laser surgery," Lasers in Surgery and Medicine 44(10), 815–823 (2012).
28. M. Narisawa, "Silicone resin applications for ceramic precursors and composites," Materials 3(6), 3518–3536 (2010).
29. G. L. Harris (Ed.), Properties of silicon carbide, INSPEC, the Institution of Electrical Engineers, London, United Kingdom (1995). ISBN: 0-85296-870-1
30. S. Hayashi, K. Tsunemitsu, and M. Terakawa, "Laser Direct Writing of Graphene Quantum Dots inside a Transparent Polymer," Nano Letters 22(2), 775–782 (2021).
31. Y. S. Park, SiC materials and devices, Semiconductors and Semimetals, vol. 52, R. K. Willardson, E. R. Weber and Y. S. Park (Ed.), Academic Press (1998). ISBN 978-0-12-752160-2
32. Z. G. Mohammadsalih, N. S. Sadeq, "Structure and properties of polystyrene/graphene oxide nanocomposites," Fullerenes, Nanotubes and Carbon Nanostructures 30(3), 373–384 (2021).
33. A. J. Gordon, R. A. Ford, The chemist's companion: a handbook of practical data, techniques, and references, John Wiley & Sons (1972). ISBN: 0-471-31590-7
34. A. N. Lazarev, I. S. Ignat'ev, and T. F. Tenisheva, "Vibrations of Simple Molecules with SiO Bonds", Nauka Publishers, Leningrad, 159 (1980). [in Russian]
35. R. Kitamura, L. Pilon, and M. Jonasz, "Optical constants of silica glass from extreme ultraviolet to far infrared at near room temperature," Applied Optics 46(33), 8118–8133 (2007).
36. L. Yanjie, O. Jun, W. Hongyou, W. Weili, C. Pengfei, and S. Kangning, "Synthesis and characterization of core–shell structured SiO_2@YVO4:Yb^{3+}, Er^{3+} microspheres," Applied Surface Science 258(8), 3689–3694 (2012).